Quantitative coal mineralogy of the Sydney Coalfield, Nova Scotia, Canada, by scanning electron microscopy, computerized image analysis, and energy-dispersive X-ray spectrometry

DIETER BIRK[1]
Geofuel Research Inc., Box 1324, Sydney, N.S., Canada B1P 6K3

Received February 13, 1989
Revision accepted October 16, 1989

Automated image and X-ray analysis, with a scanning electron microscope, has been used to "fingerprint" mineral particles in bituminous coals of the Sydney Coalfield and catalogue their chemical class and size distribution. Four seams (Hub, Harbour, Phalen, and Gardiner) were analyzed quantitatively for some 32 000 mineral particles; these analyses revealed particle-size and weight distributions for 27 chemical classes. Manual searches augmented the computer-automated scans, covering eight seams and recording a total of 35 mineral species, their paragenesis, and sites for 28 elements.

Sydney seam mineralogy is dominated by pyrite and kaolinite, but illite, chlorite, siderite, ankerite, and quartz are locally prominent; these are accompanied by a large variety of accessory minerals (zircon, rutile, apatite, barite, gypsum, rare-earth phosphates, and ore minerals) and alteration products (goethite and hydrated sulphates). Individual column benches show geochemical facies with different mineral suites resulting from cyclic sedimentation, hydrologic conditions, and changes in pore-water chemistry during peat accumulation, coalification, and diagenesis. A sulphide facies and a siderite–chlorite facies are recognized within one seam (Harbour); these facies change vertically and laterally within lithotype bands.

Stratigraphic correlation is precluded, but quantitative mineralogy can elucidate paleoenvironments and be applied to coal-cleaning technology (beneficiation) or environmental studies.

L'analyse d'images automatisée et d'énergie dispersive des rayons-X, avec un microscope électronique à balayage, a servi à caractériser les particules minérales dans les charbons bitumineux du bassin houiller de Sydney et en plus à cataloguer leur classe chimique et leur distribution granulométrique. Les analyses quantitatives de quelque 32 000 particules minérales dans quatre couches de charbon (Hub, Harbour, Phalen et Gardiner) ont dévoilé l'existence de 27 classes de grosseur de particules et de répartitions pondérales. Des opérations manuelles ont permis d'obtenir des balayages automatisés améliorés, couvrant huit couches de charbon, ce qui a autorisé l'identification en tout de 35 espèces minérales, l'établissement de leur paragenèse et la localisation des sites qu'occupent 28 éléments.

La minéralogie des couches de charbon comprend surtout de la pyrite et de la kaolinite, mais les minéraux illite, chlorite, sidérite, ankérite et quartz sont localement abondants et accompagnés d'un cortège varié de minéraux accessoires (zircon, rutile, apatite, barite, gypse, phosphates de terres rares et minéraux métalliques) et aussi de produits d'altération (goethite et sulfates hydratés). La stratigraphie des bancs individuels montre des faciès géochimiques caractérisés par des assemblages minéralogiques différents dus à la sédimentation cyclique, aux conditions hydrologiques et aux variations de la composition chimique de l'eau des pores durant l'accumulation de la matière végétale, la transformation en charbon et la diagenèse. Un faciès à sulfures et un faciès à sidérite–chlorite sont reconnus dans une couche de charbon (Harbour); ils varient verticalement et latéralement à l'intérieur des lithotypes.

Les corrélations stratigraphiques sont impracticables, cependant la minéralogie quantitative peut fournir des enseignements sur les paléomilieux et peut être appliquée dans la technologie de purification (enrichissement) ou dans les études d'impact environnemental.

[Traduit par la revue]

Can. J. Earth Sci. **27**, 163–179 (1990)

Introduction

Commercial coal mining was first activated at Morien Bay in the Sydney Coalfield when colonialists of Fortress Louisbourg shipped coal from the Harbour seam to France in 1724. They recognized ubiquitous "sulphuret of iron" (pyrite) and "carbonates of lime and iron" (calcite and siderite), which the first studies (Dawson 1859) attributed to impregnation from adjacent lithology.

Difficulties in analyzing for these microscopic inclusions have been discussed by Finkelman and Gluskoter (1981) and documented by interlaboratory round robins (Finkelman *et al.* 1984; Vleeskens and Hamburg 1987). Because of such analytical limitations, the nature of coal minerals in the Sydney Coalfield has received scant attention, in contrast with maceral petrography.

Our study, using recent advances in computer-automated image analysis (AIA), scanning electron microscopy (SEM), and energy-dispersive X-ray spectrometry (EDX), addresses the mineralogy question. Coal microstructure, mineral morphology, and trace-element sites are readily discerned by SEM–EDX when back-scattered electron imaging (BEI) on polished grain mounts is used. The addition of image-analysis technology allows quantitative coal mineralogy to be determined (Huggins *et al.* 1980, 1982; Hamburg 1984; Birk 1989).

Computer-automated SEM–EDX was first developed by Pennsylvania State University to characterize minerals in coal-mine dust and, subsequently, polished coal-grain mounts (Dinger and White 1976). Researchers at U.S. Steel Corporation (Lee *et al.* 1978; Huggins *et al.* 1980, 1982) refined the mineral-particulate method and wrote specific software (Coal Mineral Analysis (CMA)). A similar particle-by-particle characterization was adopted by Straszheim and Markuszewski (1984, 1985).

Comparative data by X-ray diffraction (XRD) and SEM–EDX–AIA (i.e., CMA) reported by Finkelman *et al.* (1984) showed large discrepancies between laboratories and techniques. These errors are attributable to the absence of standardized methodology and the "constant-sum problem" inherent to geochemical percentage data (Skala 1979). Birk (1989) reviewed

[1]Present address: Suite 20, 2885 Sherwood Heights Dr., Oakville, Ont., Canada L6J 7HI.

the limitations of CMA and discussed statistical and analytical factors for quantitative mineralogy.

Previous work: Sydney Coalfield

The Sydney Basin contains 2 km of Carboniferous coal-bearing terrestrial strata of the Morien Group lying uncomformably on marine Windsor sediments (Rust *et al.* 1987). Some 16 bituminous seams are recognized; their depositional facies have been described by Hacquebard and Donaldson (1969).

The economic coals of the upper Morien (Sydney Mines Formation) were deposited under fluviolacustrine conditions in a floodplain environment (Hacquebard and Donaldson 1969). Rust *et al.* (1987) postulated peat swamps in large flood basins between unconfined channels of large meandering rivers. Northeast-trending paleoriver channels have been mapped in the submarine mine workings (Forgeron *et al.* 1986). Zodrow (1983) described the geochemistry of seam roof rocks, which consist mainly of lutites and siltstones between sandstone channels.

Petrographic and geological studies have reported 10 indigenous minerals in Sydney coals: pyrite, calcite, siderite, gypsum, chalcopyrite, marcasite, quartz, feldspar, muscovite, and kaolinite (Dawson 1859; Newman 1935; Hacquebard *et al.* 1965; Cameron 1971; Hacquebard and Avery 1982; Zodrow and McCandlish 1980). In addition, a complex suite of hydrated sulphates, derived from pyrite and marcasite decomposition, was catalogued by Zodrow *et al.* (1979) and Zodrow (1980). Mineral enrichments at seam tops and bottoms were reported by several authors (Newman 1935; Hacquebard and Avery 1982), but no quantitative studies were attempted.

The first application of electron microscopy to Sydney coals addressed the role of pyrite in coal beneficiation (i.e., washability). Walsh *et al.* (1969) used an electron microprobe to analyze pyrite from Harbour seam coal (No. 26 colliery), and they were the first to measure organic sulphur content directly as part of washability and fines-agglomeration tests. Capes *et al.* (1979) used SEM on pyrites from Prince mine (Hub seam) to study oxidation.

Analytical procedures

Four commercial coals within the Sydney Mines Formation were analyzed in detail: Hub seam (Prince colliery), Harbour seam (Lingan colliery and Donkin–Morien development), Phalen seam (Phalen colliery), and Gardiner seam (Novaco open pit). Descriptive SEM surveys were conducted on these coals and four other seams: Point Aconi, Lloyd Cove, Emery, and Mullins.

Coal samples were collected in mine workings and open pits as columnar benches or as stored core and bulk sections (Donkin–Morien). Representative splits were stage crushed to −20 mesh, mounted as 25 mm pellets (60% acrylic lucite), then polished by petrographic procedures and carbon coated.

A Jeol JSM-T300 scanning electron microscope with a BEI detector was equipped for digital beam control. Major-element X-ray spectra were monitored with a Tracor Northern 5500 microanalyzer. For manual surveys, EDX spectra were collected in spot mode for 50 s, but automated SEM–EDX–AIA used variable collection times (1–3 s).

For SEM–EDX–AIA, we used the CMA software developed by Huggins *et al.* (1980, 1982). The CMA method relied on particulate recognition by the bright BEI for minerals (in contrast with weak signals for macerals or mounting media). The sizes of mineral particulates were determined *in situ* by the electron beam. Using 11 EDX peak intensities, we grouped the particulates into 27 chemical classes, including 17 discrete minerals, eight mixtures, and two unknowns. Our software version (CMA-2A) was modified from that used by Hamburg (1984). Spectral acquisition was increased for submicrometre particles (from 1.3 s to 3 s), and X-rays were collected along particle diagonals instead of at centroids.

Mineral particles were detected at three SEM magnifications and categorized into six size bins. Individual mineral particles were sized by the electron beam along four diagonals (Lee and Kelly 1980; Hamburg 1984), from which CMA calculated the area and weight percentages. Site statistics were standardized for magnification, beam spacing, and bin sizes.

At 50× magnification the SEM scan field covered a pellet area of 3.23×10^6 μm^2 and monitored the 10–50 μm diameter particles. Scans at higher magnification (150× and 500×) searched for smaller particles (1–2.5 and 0.2–1.0 μm, respectively) and covered proportionately smaller areas but usually required more fields to reach particle counts.

Run parameters generally followed the software "default" settings, and particle recognition was based on a lower threshold of the BEI video signal, set slightly above a maceral background. Additional factors affecting computerized mineral analysis were discussed previously (Birk 1989).

For this study, the mineral varieties were grouped as chemically distinct species, emphasizing the more commonly reported isomers. Mineral identifications were based on major-element EDX spectra matched to characteristic patterns reported by McCrone and Delly (1973), Huggins *et al.* (1980), and Welton (1984) or predicted from mineral formulae. Quantitative mineralogy used the 27 chemical classes of Huggins *et al.* (1980), which are based on common occurrences in United States coals.

Because of the statistical correlation of percentage data (constant-sum problem), even one change in mineral class or elemental range can affect the entire analysis. Our data are compatible with other CMA results (Huggins *et al.* 1980, 1982; Hamburg 1984) but not with the chemical classes of Straszheim and Markuszewski (1984, 1985).

This paper compiles weight percentage data by reassigning "mixed" categories proportionally to recognized mineral classes and normalizing the sums (Birk 1989). Some authors correct for a nonproportional pyrite signal (Huggins *et al.* 1982), but we agree with Straszheim and Markuszewski (1985) that this is not always justified.

Two sets of control samples were analyzed: three coals supplied by Energieonderzoek Centrum Nederland (ECN) (Vleeskens and Hamburg 1987) and a set of "synthetic coal" standards prepared from graphite and XRD mineral standards (Chemplex Industries Incorporated, New York). The synthetic standards confirmed that major minerals were correctly identified by CMA but also revealed that the mineral powders were not homogeneous. Results for the ECN coals were within the round-robin spread.

Field observations

The columnar benches represent complete vertical seam sections (15 cm × 15 cm) from roof to underclay. All coals exhibited laminations of bright and dull bands of lithotypes (vitrain, clarain, durain, and fusain), occasionally intercalated with clay or claystone partings. Contacts were sharp against

partings and sandstone roof but gradational (as coaly shale) against clay roof. Underclays at Phalen and Hub showed visible rootlets, indicative of autochthonous coal.

Forgeron *et al.* (1986) pointed out that sulphur content of a coal seam increases adjacent to "stone bands" (i.e., shale partings) and overlying sandstone paleochannels. The visible pyrite in our collected sections corroborates this: a Hub section, overlain by sandstone, showed pyrite as cleat linings throughout and visible carbonates and gypsum at the base; a second Hub section, beneath shale, exhibited visible pyrite in top and basal benches but only traces in the centre. Likewise, the Phalen coal beneath sandstone showed prominent pyrite and calcite on cleat faces throughout the section, but beneath a shale roof, pyrite was concentrated in the bottom benches, although calcite was logged throughout. A Harbour section beneath sandstone at Lingan showed cleat pyrite midway and at the base: a shale-capped section revealed megascopic pyrite at the top and near the base.

At the Gardiner open-pit and other outcrop exposures, pyrite "sulphur balls" and irregular "beds" and clay partings could be mapped for several metres. Capping the coal was a layer of fossiliferous grey shale, filled with coalified compression flora and overlain by unconsolidated overburden.

Weathered exposures have variable degrees of pyrite alteration, siderite replacement, or pseudomorphic goethite. At Point Aconi, the cliff exposures show yellow and orange "blooms" of hydrated sulphates (sideronatrite and copiapite; Zodrow 1980) coating the coal and reddish brown iron oxides bleeding from drainage conduits. The overlying shales carry inch-size nuggets of siderite and pyrite and layers rich in compression fossils.

Results

Manual SEM–EDX survey

BEI's of polished coal grains reveal mineral–maceral intensity contrasts in the following order: heavy minerals > pyrite > goethite > rutile > siderite> chlorite > calcite > illite > quartz > kaolinite > lucite mount > macerals (Figs. 1–4). This correlates with the calculated back-scattering coefficients of White *et al.* (1984). EDX spectra from mineral grains greater than 1 μm diameter are reproducible, unless pellet surface relief influences X-ray collection. Spectra from smaller grains, inclusions, or thin films of soluble minerals (halite, gypsum) usually include interference peaks from matrix or adjacent minerals.

EDX spectra obtained on macerals yield low counts and a large Bremsstrahlung background. Spectra profiles for macerals differ within seams as much as between seams, with spectral shape controlled by the relative size of element peaks in the following order of abundance: S > Al > Cl > Ca > K, Ti. The concentrations of Si, Fe, and Cu are less certain at such low count rates because of spurious instrument peaks.

The method of analyzing channel benches as crushed grain mounts yields varying mixtures of dull and bright coal in each pellet. Bright coal (vitrain) requires a maximum contrast BEI setting at high magnification to reveal finely dispersed, low concentrations of phyllosilicates dominated by kaolinite, illite or chlorite and with lesser quartz, carbonates, and pyrite in a maceral matrix. Dull coal (duroclarain) and fusain reveal higher concentrations and more diverse mineralogy even at low magnifications. These are typified by carbominerite grains with bedded illite, quartz, and varying amounts of kaolinite, pyrite, and accessory minerals concordant to bedding (Fig. 1) or by "hard fusain" with minerals filling cell lumen (Fig. 2). Megascopic patches of pyrite ("sulphur balls") in polished section reveal carbopyrite grains consisting of pyrite cell casts, pyritized fossils, lone framboids, or framboid clusters. Individual framboids are about 10–20 μm in diameter but consist of micrometre-size octahedra. In low-sulphur coal, pyrite is absent or occurs as rare octahedra and cubes dispersed in macerals.

A multistage paragenesis for pyrite is indicated by its morphology and associations (Table 1). Syngenetic pyrite framboids and crystallite clusters associated with clay bedding show crystalloblastesis (Fig. 3). Massive pyrite casts or globules, in low-contrast BEI mode, reveal euhedral crystals cemented by second-stage pyrite or marcasite (Fig. 4). Elsewhere, pyrite forms rosettes and needle clusters within "clean" coal grains, suggesting limited nucleation and rapid crystallization. These rods weather preferentially and often display sulphur depletion. A late syngenetic stage is evidenced by pyrite framboid overgrowths or replacement of kaolinite and carbonate cell fillings. The epigenetic stage of pyritization, evident in outcrop as cleat linings, is observed microscopically as rare fracture fillings or more commonly as angular blocks of pyrite isolated in the lucite mount.

The clays show both detrital and authigenic textures. Carbargillite beds carry a single clay species or clay pairs (illite–kaolinite; kaolinite–chlorite; illite–chlorite), but often in separate bands. Kaolinite occurs alone or with abundant quartz in detrital laminations. Kaolinite is also common as authigenic growths of mealy masses or cryptocrystalline aggregates, interstitial to pyrite crystallites or filling fusinite cells (Fig. 2) and maceral breccia. Colloform "graupen" textures and fracture fillings were found only in Phalen coal.

In bright coal, kaolinite in the absence of pyrite grades into ferriferous chlorite (chamosite) either in juxtaposition or as a mixed-layer clay infilling cell lumen and dispersed throughout macerals. Illite is largely detrital and is concordant to bedding as micaceous rods or as fibrous mats and floccules draped over framboids (Fig. 3). Mixed-layer clays may be signified by the considerable chemical diversity of the illite group: notably, aluminium depletion and (or) titanium substitution and variable Ti/K ratios. The titaniferous variety is rare and randomly distributed; it is more common in the finer groundmass. Since Ti substitution in muscovite is directly proportional to metamorphic grade (Kwak 1968), these illites may be derivatives from metamorphic terrane.

For some clay flakes, the BEI shows distinct chemical layering or mottled texture correlating with variable Fe or K in EDX spectra. This can be interpreted as mixed-layer clays of kaolinite–chlorite or kaolinite–illite, similar to the intergrowths reported by White *et al.* (1984).

Quartz is common as subrounded detrital grains in carbargillite but is rarely dominant. Grains sometimes carry heavy-mineral inclusions (zircon, rutile) indicative of igneous parentage.

Carbonates are sparse in most samples and are generally associated with cleat fill; less commonly, they are present as cell casts. Calcite, grading to ankerite, is the dominant carbonate and can be associated with either abundant pyrite or siderite. Siderite occurs as cell fillings or is pseudomorphic after pyrite and usually shows trace Ca and Mn. This mineral forms abundant egg-size nodules in roof clays but appears to have limited distribution within the coals: it is usually associated with chlorite and a scarcity of pyrite.

Evaporite minerals (halite, gypsum) are present in several

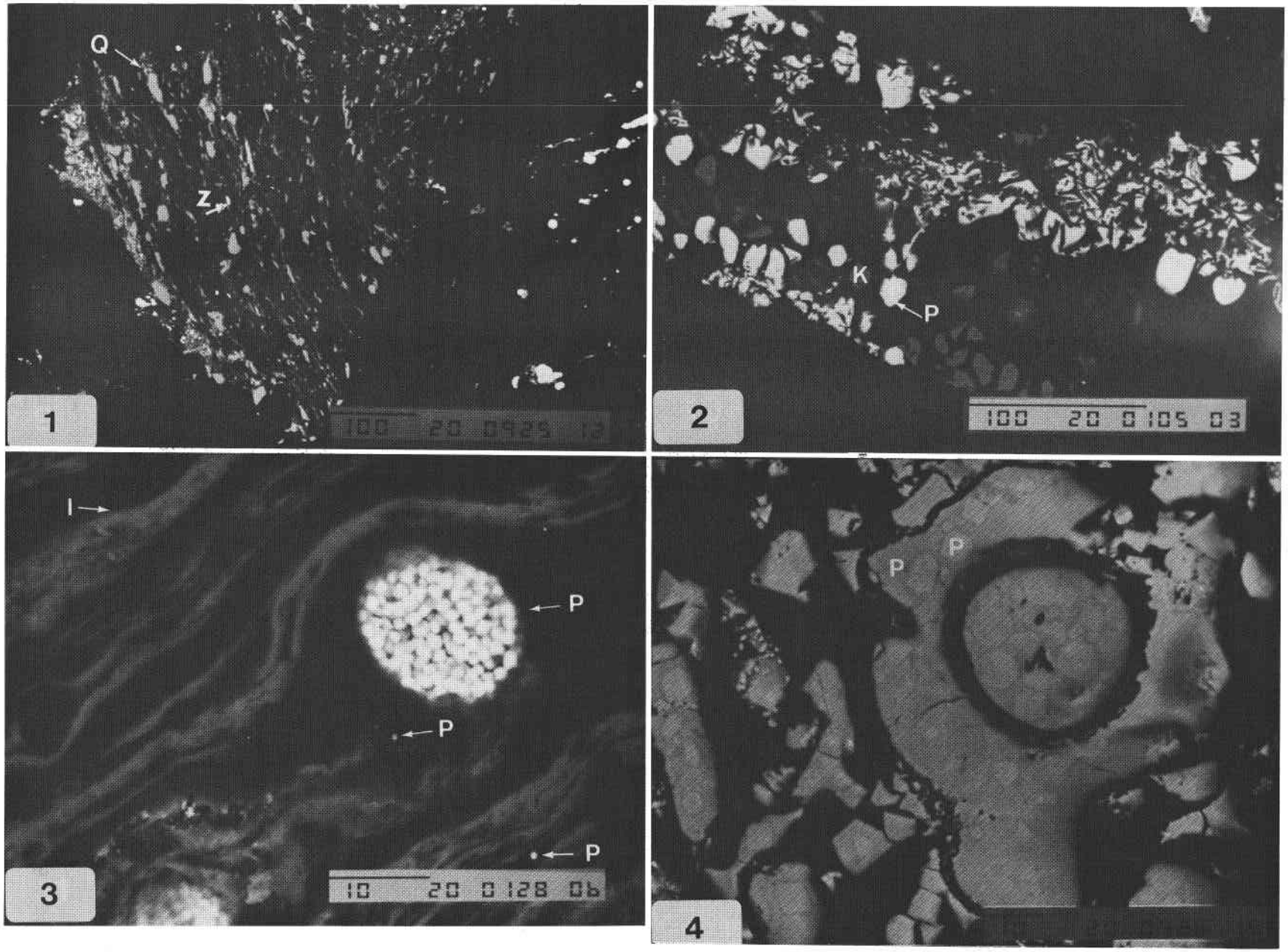

FIGS. 1–4. Photomicrographs. Information blocks give scale (bar in micrometres), excitation energy (20 keV), and catalogue number. (1) Carbominerite grain (Harbour seam). Viewed in BEI at 150× magnification, after being mounted in lucite, polished, and carbon coated. BEI brightness is proportional to average atomic number: minerals (Z, zircon; Q, quartz) are bright, contrasting against dark lucite and darker coal. (2) Fusinite cells (Mullins seam) filled by pyrite (P) and kaolinite (K). Collapsed cell walls form "bogen" textures at centre right. Loose apatite grain (A), upper right. 2000×, BEI. (3) Pyrite framboid and lone crystals (P) in carbargillite bedding (Mullins seam). Illite (I) drape texture is likely due to blastic growth at syngenetic stage of coalification 2000×, BEI. (4) Massive pyrite (P) or marcasite, pseudomorphic after botanical structure (Harbour seam). Note internal crystals and pyritic overgrowth. 1000×, BEI.

TABLE 1. Mineral paragenesis in the Sydney Coalfield

Syngenetic		Epigenetic	
Detrital	Diagenetic (authigenic)	Cleat minerals	Secondary weathering
Illite (2 types)	EARLY	Pyrite, kaolinite	Hydrated sulphates
Quartz	Pyrite framboid blasts	Calcite or ankerite	Goethite
Chlorite, kaolinite	Kaolinite, chlorite precipitates in beds	Gypsum, halite	Sulphur
Apatite (fossil)	LATE	Sulphides	Kaolinite
Rutile	Pyrite overgrowths	Chalcopyrite, sphalerite	
Zircon	Kaolinite, pyrite, chlorite cell fillings		
Monazite	Siderite		
Xenotime	Calcite or ankerite		
Barite	Halite, gypsum		
Cassiterite	Sulphides		
Inclusions	Sphalerite, chalcopyrite, galena		
Millerite, rutile			

seams, notably in Phalen, where macerals also show strong chlorine peaks. However, these minerals are partially removed by the coal-pelleting process and therefore are underestimated by an SEM survey.

Phosphates occur sparsely as detrital grains in carbominerite, but at the top of the Harbour seam, massive apatite is abundant, likely as fossil casts. Fluorine cannot be detected by our SEM–EDX system, but chlorine peaks are often present. Rare-earth phosphates (monazite, xenotime, florencite) with variable chemistry (e.g., thorium-rich monazite; xenotime with variable P/Y) occur as tiny grains in detrital layers.

The abundance of heavy minerals in the carbargillite fines is not apparent at normal BEI settings but shows up when contrast settings are minimized. Rutile is the most prolific and is visible in groundmass down to submicrometre sizes. Heavy minerals in carbominerite bedding show subrounded morphology indicative of a clastic provenance from reworked granitoids (e.g., zircon, monazite) or Windsor Group evaporites (e.g., barite, cassiterite).

Occasionally, microcrystals of sulphides or oxides (galena, sphalerite, millerite, chalcopyrite, rutile) occur within macerals or as inclusions within pyrite or quartz. Rutile inclusions in illite may be partially responsible for the titaniferous illite spectra. Such inclusions could be inherited or formed during diagenesis.

Table 2 lists all the minerals identified as well as the elements identified in macerals. Our EDX spectra of mineral grains detected 28 elements; macerals contained nine elements, not including C, H, N, and O (not monitored). Thirty primary minerals were observed; of these six are major components. At least three secondary minerals occur *in situ*.

Quantitative mineralogy: SEM–EDX–AIA

CMA runs on Sydney coals are illustrated in Figs. 5–12 and summarized in Appendix Tables A1–A5. Channel bench samples were analyzed individually (Table 3) for about 600 mineral particles each, but modal mineralogy was based on seam composites.

Of 33 minerals reported in our manual SEM survey, 13 are included in the CMA programme. All major minerals are accounted for, but minor minerals such as zircon, monazite, xenotime, cassiterite, and sphalerite are overlooked. Titanium-bearing illite is misfiled by CMA as an "unknown". Likewise, CMA cannot accommodate the variable chemistry of mixed-layer clays.

Our manual surveys were not able to verify two of the CMA mineral classes: sylvite and jarosite. The "sylvite", we suspect, is a contaminant (surface dust revealed complex Cl, K, Si, Al, S, and Fe spectra). The chemistry of jarosite, $(Na,K)Fe_3(SO_4)_2(OH)_6$, was not encountered in manual surveys.

The variety of sulphate–sulphide classes reported by CMA reflects pellet topography more than weathering in these coals. Unspecified categories (mixed, nonintegrated, and unknown) represent a large percentage of the particles encountered, especially for submicrometre sizes. When particle-by-particle chemistries are reviewed, "mixed" silicates are attributable to quartz–clay intergrowths, mixed-layer clays, or spectral interference. The "unknown" category covers compositional ratios beyond the other classes and is attributable to polishing contaminants (alumina), element substitution (e.g., Cl in apatite), or missing mineral categories in the CMA programme. The "nonintegrated" category includes substrate backgrounds and can be partially filtered out if the BEI threshold is raised, but at the expense of clay-particle recognition.

Particles smaller than the electron-beam excitation volume produce insufficient BEI contrast or mixed EDX mineral–substrate spectra and therefore are ignored by CMA or are incorrectly classified. Mixed categories are therefore reported as dominant in the smallest size bin. The stronger BEI signal for pyrite may result in less of a drop-off in the smallest bin size than for kaolinite (Figs. 6, 7). Compare this, however, with pyrite size distribution reported by Laskowski *et al.* (1985) for Prince mine coal. They also showed gradual depletion of pyrite counts below 4 μm, based on image analysis, (see our Figs. 6, 8).

Clastic sediments commonly reveal a lognormal grain-size distribution, as measured by sieve analysis or settling velocity. Microscopic sectioning techniques, on the other hand, reveal only apparent sizes, i.e., two-dimensional distributions of three-dimensional size populations. Our coal-mineral results represent such section-size data (Figs. 5–8).

Appendix Tables A1–A5 show percentage size distributions for each mineral class. At each SEM magnification, only particles of two size bins were monitored by the CMA pro-

TABLE 2. Minerals and trace elements encountered during manual SEM–EDX surveys

	EDX element sites[a]		Seams[b]							
	Major	Trace	PA	LC	Hu	Hr	Ph	Em	Ga	Mu
Major minerals										
Quartz	Si		m	m	m	m	M*	m	m	m
Pyrite	Fe,S	As,Cu	M*	M*	M*	M*	M*	M*	M*	M*
Illite	Si,Al,K,Fe,Ti		m	M	m	M	m	m	m	m
Kaolinite	Al,Si	Fe	M	M	M	M	M	M	M	M
Chlorite	Si,Fe,Al,Mg	Mn,Ti,Cu	—	—	t	M	t	t	—	—
Mixed clay	Si,Al,Fe,K	Na,Ti	m	m	m	m	m	m	m	m
Montmorillonite	Si,Al,K,Fe,Na		—	—	—	—	t	—	—	—
Calcite	Ca	Fe,Mg,Mn	—	—	*	m	M*	—	—	—
Dolomite	Ca,Mg	Fe,Mn,Cl	—	—	—	m	t	—	—	—
Ankerite	Ca,Fe	Mn,Mg,Cl	—	—	t	M*	—	—	—	—
Siderite	Fe	Ca,Mn	—	—	*	M*	t	—	t	—
Accessory minerals										
Biotite	Si,Fe,K,Al	Ti,Mn,Mg	—	—	—	t	—	—	t	—
Zircon	Si,Zr	Ti,Ce	t	—	—	t	—	t	t	t
Rutile	Ti		t	t	t	t	t	t	t	t
Ilmenite	Fe,Ti	Cu	—	—	—	—	—	—	t	—
Apatite	Ca,P	Cl,Yb	—	—	—	m	t	—	—	—
Monazite	Ce,P,Th,Si	La,Ca	t	—	t	t	t	t	t	t
Florencite(?)	P,Al,Ce,Sr,Ca,Ba	Fe,K	t	—	t	—	t	—	—	t
Xenotime	P,Y	Gd,Yb,Er(?)	—	—	—	t	t	t	—	—
Gypsum	S,Ca	Cl	—	—	*	*	t*	—	—	—
Halite	Cl,Na		—	t	—	—	t*	—	t	—
Barite	Ba,S		t	—	—	—	t	t	t	—
Chalcopyrite	S,Fe,Cu		t*	—	—	t*	—	t	t	—
Arsenopyrite	Fe,S,As		—	—	—	—	—	—	m	—
Sphalerite	S,Zn	Cu	t	—	—	—	t	t	—	t
Galena	S,Pb		*	t*	—	t	—	—	t	t
Millerite	Ni,S		—	—	—	t	—	—	—	—
Cassiterite	Sn		—	—	—	t	—	—	—	—
Tennantite(?)	S,Fe,Cu,Zn		—	—	—	—	—	t	—	—
Almandite(?)	Fe,Si,Al	Cu	—	—	t	t	—	—	—	—
Gibbsite(?)	Al		—	t	—	t	—	—	—	—
Secondary minerals										
Sulphur	S		—	—	—	—	—	t	—	t
Goethite	Fe		*	*	—	t	—	*	t*	—
Copiapite(?)	S,Fe	Al,Mg,K	*	t	—	t	—	t	—	—
Coal macerals	S,Fe,Si,Al		M	M	M	M	M	M	M	M
		Ti	—	t	—	t	—	t	t	t
		K	—	—	—	t	—	—	t	t
		Ca	m	t	t	m	m	m	m	m
		Cl	m	m	m	m	M	m	m	m
		Br	—	t	t	—	—	—	—	—
		Cu	—	t	t	t	t	—	—	t

NOTE: (?), identity uncertain.

[a]Elements below atomic No. 11 (C, H, N, O, F, B, Be, and Li) not monitored. Artifacts from SEM contribute Cu, Fe, Al, and Si.

[b]Seams in descending stratigraphic order: PA, Point Aconi; LC, Lloyd Cove; Hu, Hub; Hr, Harbour; Ph, Phalen; Em, Emery; Ga, Gardiner; Mu, Mullins. Identification by EDX element: M, major; m, minor; t, trace; *, reported visually (megascopic); —, not detected.

gramme. The raw particle counts show bimodal distributions that are a function of this pairwise sampling. There are always more fines than coarse particles until the lower detection limit is reached. Such data can be recalculated to equivalent SEM areas to yield positively skewed frequencies. Thus the particle-size distributions reported in the Appendix are relative percentages normalized with respect to equivalent pellet areas.

Size distributions for six Sydney coals are compared in Fig. 5, as well as one western Canada bituminous coal (Greenhills mine, B.C., reported by Birk 1989). The western coal is characterized by greater particle frequency in the 0.2–5 μm range than the Sydney seams but has a similar depletion in numbers of larger particles.

The lowest particle densities ("cleanest" coal) are shown for the Harbour seam at Lingan (in contrast with "dirtier" Donkin coal). The two seam profiles from Lingan mine indicate that roof rock had no influence on mineral-size distribution (Fig. 5).

Individual mineral-size profiles show considerable in-seam variation. Calcite size-distribution curves show negative skew for a minor concentration of 5% in the Harbour seam (Donkin,

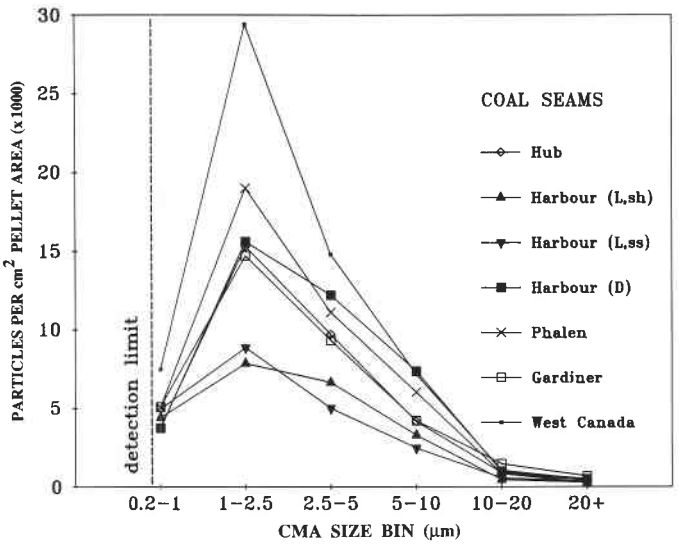

FIG. 5. CMA size distribution of coal minerals in the Sydney seams compared with that of Greenhills coal from western Canada. Normalized to equivalent pellet areas for three SEM magnifications. L, Lingan; D, Donkin; sh, shale roof; ss, sandstone roof.

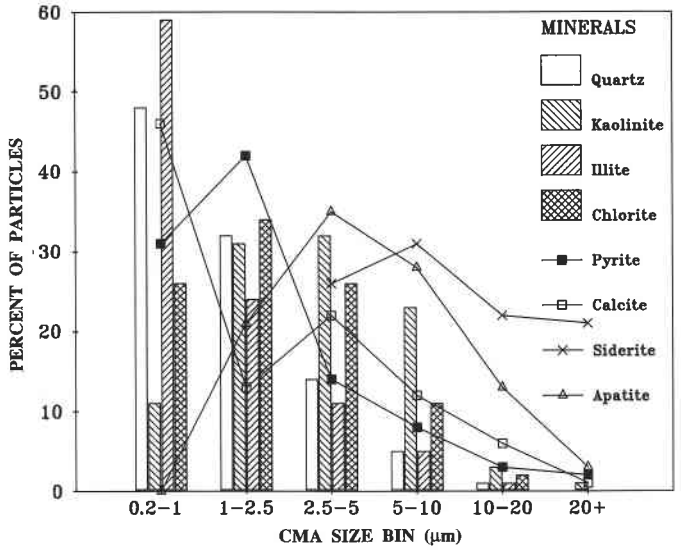

FIG. 6. CMA mineral particle sizes for the Harbour column (Lingan), collected beneath a shale roof (Appendix Table A2). Percentages pertain to each mineral class.

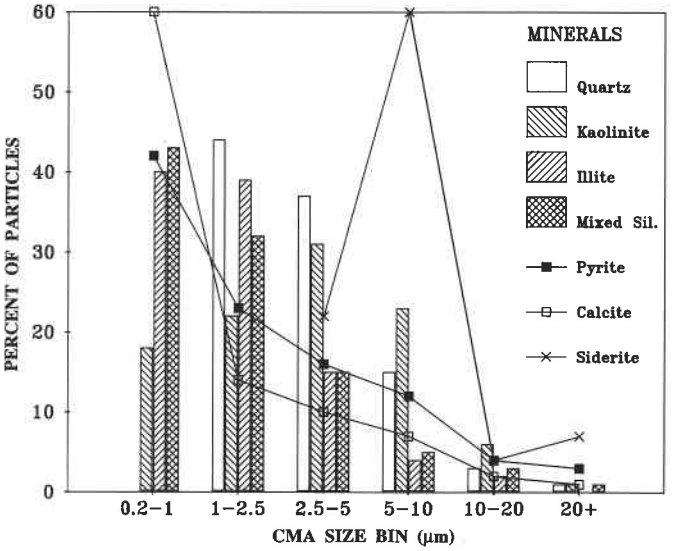

FIG. 7. CMA mineral sizes for the Harbour column (Lingan), collected beneath sandstone. Sil, silicates. Data from Birk (1989).

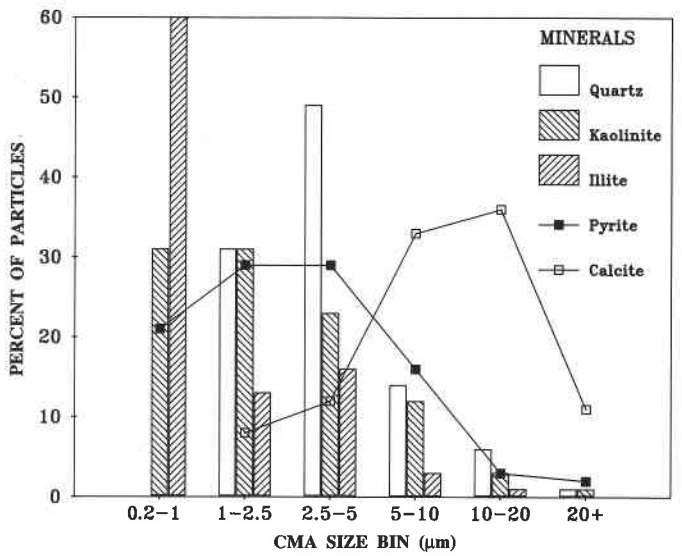

FIG. 8. CMA mineral sizes for the Harbour seam (Donkin) (Appendix Table A3).

Fig. 8), but at trace concentrations of 0.5% in the Lingan mine, calcite shows positive skew (Figs. 6, 7). This may reflect a cleat-fill versus syngenetic paragenesis.

Average mineral modes of the Sydney seams can be derived from pooled data (Table 4) and compared with CMA results for other North American bituminous coals. Relative to the Herrin No. 6 coal of Illinois or the Greenhills coal of British Columbia, Sydney coals are depleted of quartz and enriched in pyrite. The western Canadian coal has a higher kaolinite/illite ratio and less carbonate.

Discussion

Mineral suites and paragenesis

Out of approximately 100 primary minerals reported in the literature for bituminous coals, 31 have been identified in the Sydney Coalfield by this study. This suite is similar to the listing of Stanton and Finkelman (1979) and compares with the mineral suite reported for the Herrin No. 6 high-sulphur coal from Illinois (Finkelman *et al.* 1984). On the other hand, many of the mineral phases reported by Finkelman (1978) and Finkelman and Stanton (1978) for the Waynesburg coal were not recognized in our Sydney samples, likely because those authors used a greater variety of techniques. These other accessory minerals may still be discovered or may reflect geological differences in detrital minerals or pore-water chemistry.

Some workers have assumed the presence of only one clay in the Sydney coals (e.g., kaolinite: Hacquebard and Avery 1982). Our work showed that kaolinite dominates, but certain lithotype bands may carry primarily chlorite or illite and the major clays may coexist with traces of montmorillonite or mixed-layer clays.

The geochemistry of clays pertaining to sedimentation and

TABLE 3. Mineral weight percentage for columnar benches,

Sample No.[a]	Depth[b] (m)	ASTM tests[c]			CMA major minerals (wt.%)[c]								
		Ash	S	Py–S	Py	Qtz	Ill	Kao	Mx Sil	Chl	Sid	Cal	Ap
A	0.15	11.16	4.60	3.61	34.4	1.8	1.0	13.6	8.8	—	—	t	11.0
B	0.30	3.83	3.18	2.63	62.2	2.1	0.5	12.8	7.8	—	0.1	t	—
C	0.45	3.37	2.66	2.01	51.9	1.3	1.2	18.9	10.3	0.2	0.2	0.2	—
D	0.58	0.94	0.41	0.05	1.9	0.6	2.1	8.7	36.6	18.0	10.5	0.2	—
O	0.63	1.99	0.31	0.04	t	6.8	0.3	1.5	28.2	36.0	3.3	—	0.6
E	0.75	1.54	0.41	0.04	t	3.1	1.4	1.6	23.5	26.4	15.8	t	—
F	0.90	2.01	0.53	0.05	t	t	1.9	28.7	21.1	1.4	10.1	0.1	1.1
G	1.05	2.12	0.37	0.05	0.9	5.2	0.8	3.6	17.5	18.7	4.8	1.0	—
H	1.20	9.37	1.07	0.47	6.4	12.0	2.6	5.3	41.1	4.8	1.5	—	—
I	1.35	3.47	2.34	1.80	61.0	0.5	0.7	7.8	7.7	0.1	5.1	1.2	—
J	1.50	1.04	0.39	0.03	8.2	6.7	4.3	13.3	13.8	0.3	21.1	2.0	—
K	1.65	3.83	1.98	1.20	57.9	4.4	1.8	13.4	8.2	0.1	0.3	0.6	—
L	1.80	4.93	2.03	1.28	43.5	3.3	13.0	7.7	11.0	—	—	0.8	—

NOTES: About 600 particles were analyzed per bench to yield semiquantitative statistics; —, not detected; t, trace.
[a]Bench O is a basin-wide durain bed. Two mineral facies are indicated: sulphide (A–C, I–L) and siderite (D–H).
[b]Depth measured from roof rock.
[c]Ap, apatite; Cal, calcite; Chl, chlorite; Cl, chloride; Fe, iron; Gyp, gypsum; Hal, halite; Ill, illite; Jar, jarosite; Kao, kaolinite; Mont, montmorillonite; Mx, mixed; Nonin, nonintegrated; Org, organic; Py, pyrite; Qtz, quartz; Rut, rutile; S, sulphur; Sid, siderite; Sil, silicate; Sul, Sulphate; Unk, unknown. Mineral classes after Huggins *et al.* (1980).

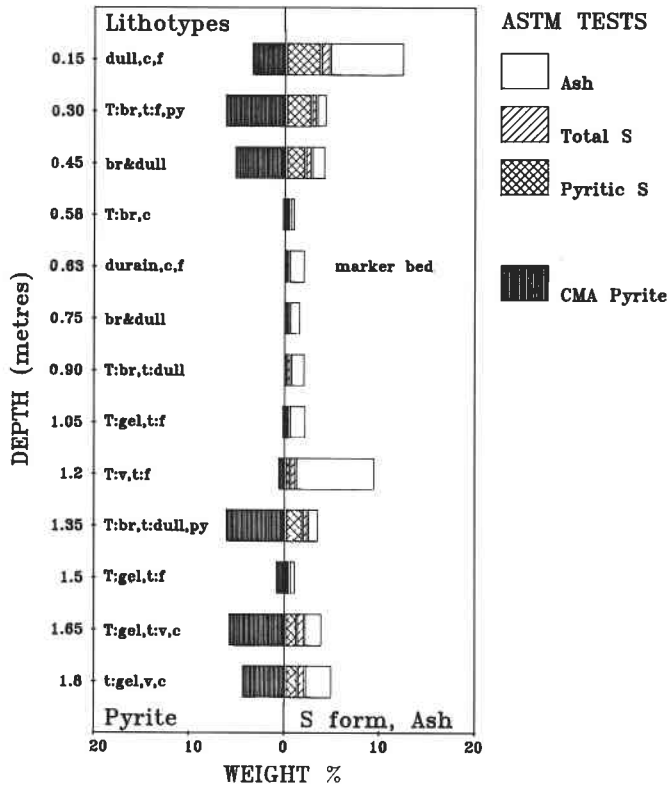

FIG. 9. Harbour seam (Lingan) profile: field descriptions and ASTM bulk tests (Table 3) correlated with pyrite content. Depths (not to scale) correspond to base of column benches, measured from shale roof. Lithotypes: br, bright; c, clarain; f, fusain; gel, gelified band, py, pyrite; T, thick band, t, thin; v, vitrain. Pyrite weight percentage is scaled to left of centre; ASTM tests are scaled to right of centre. Durain marker has been correlated basinwide.

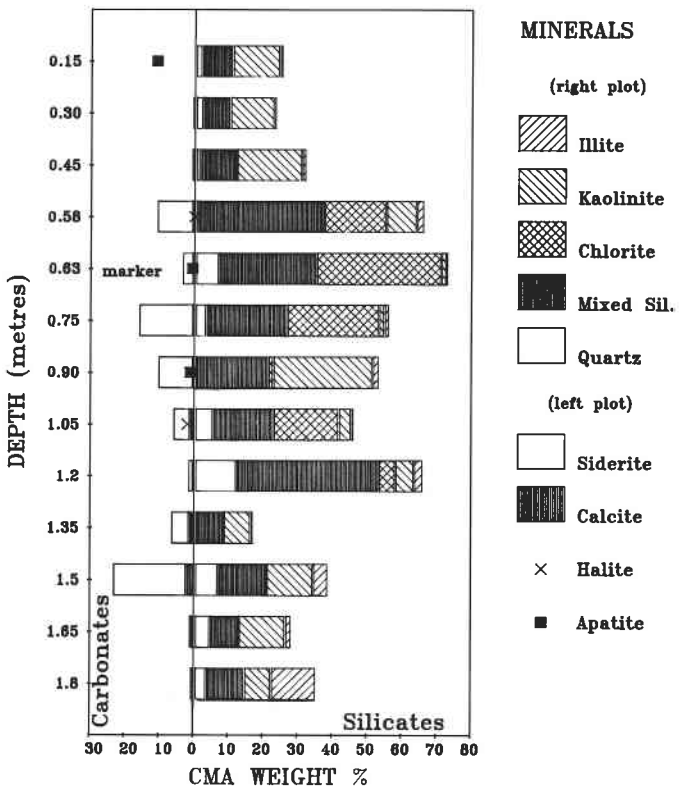

FIG. 10. Mineral profiles, Harbour seam (as in Fig. 9). Clays and iron-bearing minerals only. Data from Table 3.

diagenesis is sufficiently understood (Millot *et al.* 1970) that we can postulate paleoenvironment from present coal mineralogy. Detrital illites in dull coal lithotypes are pedogenetic, derived from sericitization of feldspars and micas from igneous sources

Harbour seam (Lingan mine), collected from shale roof

CMA unknown[c] (wt. %)		CMA sulphates[c] (wt. %)			CMA trace minerals (wt.%)[c]							
Nonin	Unk	Py–Jar	Fe Sul	Mx Sul	Hal	Mx Cl	Gyp	Rut	Qtz–Org	Qtz–Py	Org–S	Mont
13.8	4.2	0.3	7.3	0.7	—	—	—	—	1.2	1.8	—	—
2.4	0.5	t	10.9	—	t	—	—	—	0.3	0.2	—	—
5.0	2.5	0.2	5.6	—	t	—	—	—	1.5	1.0	—	—
7.4	10.8	—	—	—	0.1	0.1	—	—	2.1	1.0	—	—
7.5	14.6	—	—	—	0.8	t	0.1	0.2	0.1	—	0.1	—
7.6	18.2	—	—	—	t	—	—	—	0.9	0.9	—	0.6
4.1	22.0	—	—	—	1.4	0.5	0.1	—	5.6	1.7	—	—
13.1	29.8	—	—	—	2.0	1.1	—	0.5	0.9	0.2	—	—
17.7	6.7	0.1	0.1	t	—	—	—	0.1	0.7	0.6	—	0.5
5.2	1.0	1.8	6.5	—	—	—	—	—	0.8	0.4	t	t
21.2	4.0	0.4	1.8	—	—	—	—	—	1.7	0.9	0.2	0.3
4.7	0.4	1.5	4.5	—	—	—	—	—	1.0	0.8	t	0.4
10.8	0.1	2.2	1.3	t	—	—	—	—	3.7	2.6	—	—

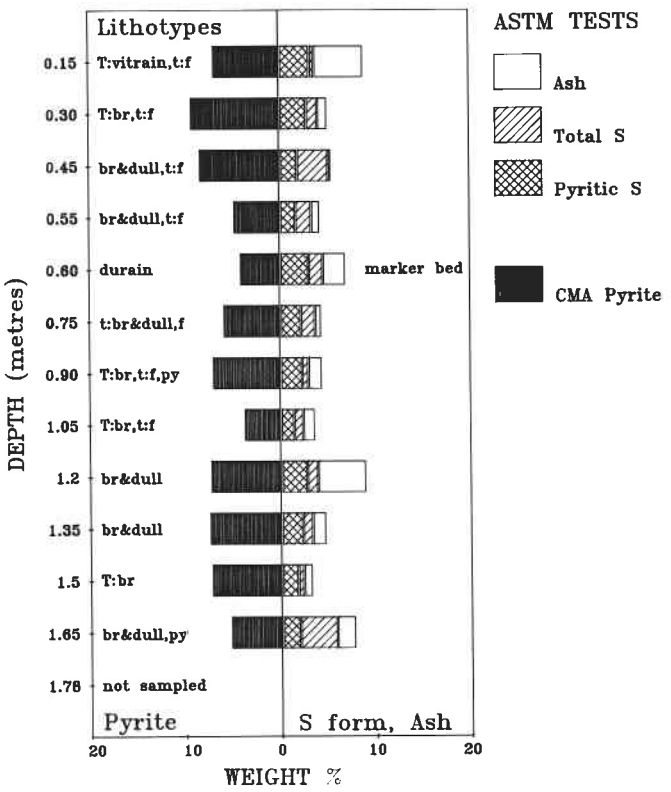

FIG. 11. Harbour seam profile, Lingan mine (sandstone roof). Data from Birk (1989). Compare marker-bed ash and sulphur forms with the equivalent horizon in Fig. 9.

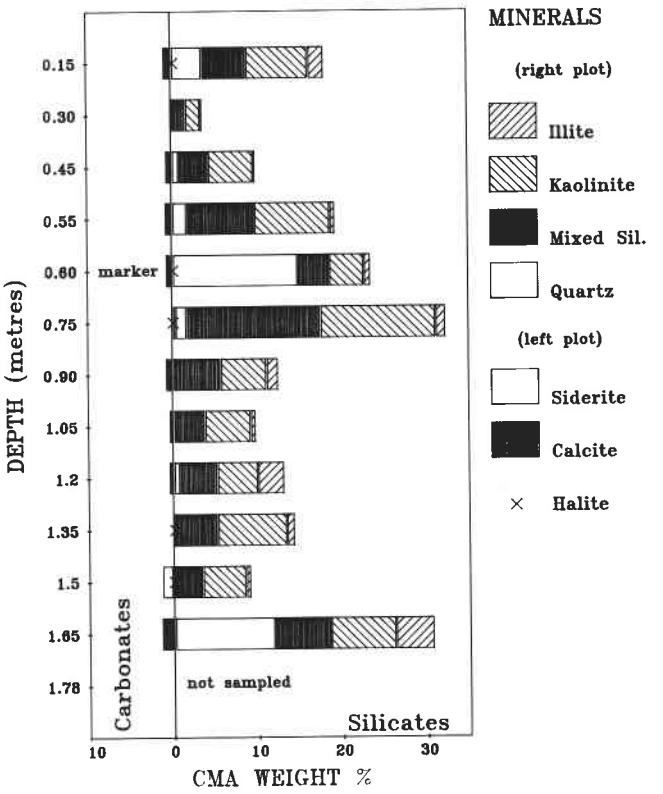

FIG. 12. Mineral profiles, Harbour seam (as in Fig. 11). The base sample was missed because of wetter conditions associated with the sandstone roof.

or reworked argillites. Interbedding of clastic clays with authigenic kaolinite suggests cyclic changes in water chemistry. Below the peat swamp, fresh water became anoxic and acidic as a result of humic acids from the organic matter, and if cation depleted, precipitated kaolinite. Where the waters were alkaline and cation rich (especially iron), neoformation of three-layer clays occurred (chlorite, illite, and montmorillonite); these three-layer clays subsequently weathered to mixed-layer clays and kaolinite.

In the absence of marine incursions in the stratigraphic section, the high sulphur content of Sydney coals has been attributed to detrital gypsum derived from river erosion of

TABLE 4. Average coal mineralogy (weight percentages) for the Sydney Coalfield seams compared with other bituminous coals, based on CMA

	Sydney Coalfield seams[a]								
	Hu	Hr sh	Hr ss	Hr D	Ph	Ga	Sydney[b]	Herrin[c]	B.C.[d]
Major									
Quartz	2.9	8.3	4.6	3.3	15.6	10.6	7.5	29.8	29.9
Kaolinite	13.7	27.2	11.8	6.4	12.5	3.6	12.5	9.6	54.1
Illite	5.7	5.5	2.4	4.2	11.6	13.1	7.1	9.0	5.5
Montmorillonite	0.2	0.2	0.2	0.2	0.9	0.7	0.4	1.3	6.9
Pyrite	68.3	37.7	75.6	75.3	43.3	61.2	60.2	36.0	0.3
Siderite	0.3	8.3	0.2	0.4	0.1	1.3	1.8	0.3	0.6
Calcite, dolomite, ankerite	0.6	0.7	0.5	5.9	10.8	—	3.1	5.5	0.3
Minor									
Gypsum	t	t	—	t	—	—	t	0.2	—
Halite	0.4	0.4	t	—	1.5	—	0.4	—	t
Sylvite	t	—	t	—	—	—	t	—	—
Apatite	—	1.5	0.1	t	0.1	—	0.3	t	1.5
Rutile	t	t	t	t	0.1	t	t	t	0.9
Chlorite	—	5.4	t	0.1	0.2	0.1	1.0	0.2	—
Secondary									
Sulphate, sulphur	7.8	4.8	4.7	4.1	3.3	9.4	5.7	8.1	—
Total	100	100	100	100	100	100	100	100	100

NOTES: Recalculated from Appendix Tables A1–A5 (mixed categories are reassigned; data are normalized); t, trace.
[a]Sydney Coalfield seams as in Table 2; sh, shale roof; ss, sandstone roof (Lingan); D, Donkin–Morien.
[b]Sydney Coalfield average coal mineralogy based on the four Sydney seams (32 063 grains).
[c]Illinois Herrin No. 6 coal minerals (Finkelman *et al.* 1984). Reported traces of jarosite, K-feldspar, sphalerite, barite, zircon, rare-earth phosphates, and rare-earth silicates. Published CMA was recalculated to remove the pyrite correction.
[d]Greenhills mine, British Columbia; average coal mineralogy based on five seams (five pellets, 2864 particles) from Birk (1989).

Windsor Group evaporites (Gibling *et al.* 1989; Rust *et al.* 1987). Portions of the swamp were thus subject to inundation by sulphate-rich river waters. Contact with acidic swamp waters created a concentration gradient and a migration of SO_4 throughout the peat. In the presence of organics and iron, bacterial sulphate reduction precipitated early-stage pyrite.

If sulphate reduction exceeds the supply of iron, H_2S is generated, making waters alkaline and causing carbonates such as calcite or dolomite to precipitate. The depletion of sulphate with excess iron would favour chlorite or siderite formation, as may have been the case in part of the Harbour seam (Fig. 10).

Nicholls (1969) defined four geochemical facies for coalfield shales and mudstones: sulphide facies, sulphide–carbonate facies, carbonate facies, and oxide facies. To simulate depositional mineralogy, he calculated an argillaceous norm but found an anomaly: normative chlorite was significantly lower for sulphide facies than for siderite facies. He proposed the presence of pH-dependent authigenic chlorite. Mineral assemblages matching two of these facies (sulphide and siderite, i.e., carbonate) are present in the Harbour seam, and both CMA and manual SEM surveys confirm the presence of chlorite, coexisting with siderite.

Sydney coal-mineral paragenesis (Table 1) suggests that diagenetic alterations during and after compaction, especially at seam edges, were fed by pore water via permeable-sandstone paleochannels. After coalification, epigenetic calcite, pyrite, and evaporites (halite and gypsum) grew in cleats as a result of groundwater leaching or seawater contamination.

Seam profiles and correlations

In Sydney seams, Hacquebard and Donaldson (1969) and Cameron (1971) mapped organic facies correlated with water depths: bright coals (vitrain, clarain) derived from forest moor (dry, terrestrial zone); dull coals (durain), from open moor (subaquatic, limnic zone); microbanded coals (fine clarain), from reed moor (transitional zone). The present study identified mineral facies that also relate to paleohydrology and lithotypes.

Clarain–durain bands are rich in carbargillite with well-bedded clastic quartz and illite. The very bright bands (vitrain) are relatively free of detrital minerals and are characterized by low quantities of authigenic clays or trace minerals. The relative permeabilities of the dull and the bright coal bands may have been responsible for subsequent differential impregnation with epigenetic pyrite, carbonates, and evaporites.

The organic facies reported for the Harbour seam differ vertically and laterally, but prominent, dull band horizons allow for basin-wide correlation. The mineralogical profile in Table 3 contains a durain band (sample O) in the Harbour seam that likely corresponds to band I of Cameron (1971) or band IV of Hacquebard and Avery (1982).

The durain marker in the shale-capped section shows unusually high chlorite contents with minor quartz and siderite (Fig. 10). Ash, total sulphur, and pyritic sulphur levels are very low. These features suggest dry deposition (free of fluvial detritus or acidic waters) and dense compaction (by desiccation?) into a layer less pervious to epigenetic mineralization. But the mineralogies above and below the durain marker are similar and do not change abruptly until high-pyrite zones are encountered, towards the roof or floor.

At the base of this section the clay is dominantly illite, but kaolinite dominates near the top. An attempt to correlate this mineralogical profile with a second section collected beneath a sandstone channel some 300 m east (Figs. 11, 12) reveals both lateral and vertical facies changes. Ash levels are markedly

higher in the body of the seam, including the durain marker. Syngenetic or epigenetic pyrite has penetrated the entire section (compared with seam top and bottom in Fig. 9), and the chlorite–siderite suite is missing. Evaporite minerals were not introduced with the sulphate-rich waters: they do not correlate with high pyrite. Halite is enriched in the chlorite–siderite zone rather than in the sulphide facies.

A third section of the Harbour seam is represented by the Donkin development, 15 km southeast. Our preliminary results (Appendix Table A3; Fig. 7) suggest a mineral facies characterized by abundant pyrite and coarse calcite. We conclude, on the basis of the lateral diversity in the Harbour seam, that stratigraphic correlation by mineralogy is unreliable.

Coal technology

This mineralogical study has application to coal mining, combustion, and conversion technology (Raask 1985). The particle-size data reveal the abundance of coal-mineral fines in the 0.2–20 μm range, which can contribute to respirable mine dust and can influence the size of combustion fly ash. Mineral-size analyses (Figs. 6, 7) show that carbonates (siderite and calcite) are present as relatively large grains and are easily isolated, compared with submicrometre size dispersed clays. Pyrite is abundant down to respirable dust sizes, diminishing at submicrometre levels.

Capes *et al.* (1979) claimed that up to 80% of pyrite could be removed by pulverizing these coals to −325 mesh (45 μm) and following this with oil agglomeration. Our evidence of micromineralogy suggests that it would be necessary to "micronize" the coal to achieve optimum pyrite removal. Ultraclean "micronized" coal may be achieved by magnetic separation because of the presence of several Fe-bearing minerals (chlorite, siderite, and goethite).

We must caution, however, that our results are limited to the <50 μm *in situ* grains. Laskowski *et al.* (1985) pointed out that pyrite distribution for the Hub seam is bimodal for coal crushed coarser than 53 μm (>270 mesh). Washability studies have shown that some 40% of Sydney coal minerals are in particles of > 300 μm diameter. These coarser minerals form the visible sulphur balls and cleat linings not adequately sampled by SEM.

Conclusions

This mineralogical study of the Sydney Coalfield revealed that variations in texture and association of minerals are as great within seams as between seams. Mineral morphology and intergrowths allow paragenetic classification into detrital, diagenetic, cleat, and secondary minerals. The multiple parentage for clays and the multiphase nature of pyrite attest to a complex history of fluid–peat and fluid–rock interaction in an open geochemical system. Coal capped by sandstone paleochannels has been more extensively pyritized than sections of the same seam overlain by shale, perhaps because the paleochannels acted as conduits for compaction fluids.

All minerals previously reported for Sydney coals have been verified by SEM–EDX except for muscovite and feldspars. These coals are dominated by pyrite and kaolinite but in places carry carbonate–chlorite, quartz–illite, or mixed-clay suites. Rutile is a common accessory. At least 35 mineral species containing over 28 elements, are present.

Quantitative mineralogy by SEM–EDX–AIA with CMA software is a valuable addition to manual SEM surveys for characterizing the mineralogical facies. CMA weight percentages can be used to map vertical or lateral changes. Particle-size information reveals clastic or diagenetic origin and predicts coal beneficiation or combustion behaviour.

Acknowledgments

This study was derived from contract research conducted by the Atlantic Coal Institute and Geofuel Research Inc. Contributions are acknowledged from Judy White, Donna McMahon, Robert O'Donnell, Alex Dove, Cassandra Birk, and Helen Costello. Thanks go to R. B. Finkelman, P. K. Mukhopadhyay, and anonym for critical reading.

Birk, D. 1989. Coal minerals: quantitative and descriptive SEM–EDX analysis. Journal of Coal Quality, **8**(2): 55–62.

Cameron, A. R. 1971. Some petrological aspects of the Harbour coal seam, Sydney Coalfield, Nova Scotia. Geological Survey of Canada, Bulletin 175.

Capes, C. E., Sproule, G. I., and Taylor, J. B. 1979. Effect of crystal structure on the removal of pyrite from coal by oil agglomeration. Fuel Processing Technology, **2**: 323–329.

Dawson, J. W. 1859. On the vegetable structures in coal. Journal of the Geological Society, London, **15**: 626–641.

Dinger, D. R., and White, E. W. 1976. Analysis of polished sections as a method for the quantitative 3-D characterization of particulate materials. Scanning Electron Microscopy, **1976** (Part III): 409–416.

Finkelman, R. B. 1978. Determination of trace element sites in the Waynesburg coal by SEM analysis of accessory minerals. Scanning Electron Microscopy, **1978** (Part I): 143–148.

Finkelman, R. B., and Gluskoter, H. J. 1981. Characterization of minerals in coal: problems and promises. *In* Fouling and slagging resulting from impurities in combustion gases. *Edited by* R. W. Bryers. Engineering Foundation, New York, pp. 299–318.

Finkelman, R. B., and Stanton, R. W. 1978. Identification and significance of accessory minerals from a bituminous coal. Fuel, **57**: 763–768.

Finkelman, R. B., Fiene, F. L., Miller, R. N., and Simon, F. O. 1984. Interlaboratory comparison of mineral constituents in a sample from the Herrin (No. 6) coal bed from Illinois. United States Geological Survey, Circular 932.

Forgeron S., MacKenzie B., and MacPherson, K. 1986. The effects of geological features on coal mining, Sydney Coalfield, Nova Scotia. CIMM Bulletin, **79** (No. 891): 79–87.

Gibling, M. R., Zentilli, M., and McCready, R. G. L. 1989. Sulphur in Pennsylvanian coals of Atlantic Canada: geologic and isotopic evidence for a bedrock evaporite source. International Journal of Coal Geology, **11**: 81–104.

Hacquebard, P. A., and Avery, M. P. 1982. Petrography of the Harbour seam in the Donkin reserve area of the Sydney Coalfield, Nova Scotia. *In* Coal: Phoenix of the 80's, Proceedings, 64th CIC Coal Symposium. *Edited by* A. M. Al Teweel. Canadian Society of Chemical Engineering, pp. 79–86.

Hacquebard, P. A., and Donaldson, J. R. 1969. Carboniferous coal deposition associated with flood-plain and limnic environments in Nova Scotia. *In* Environment of coal deposition. *Edited by* E. C. Dapples and M. E. Hopkins. Geological Society of America, Special Paper 114, pp. 141–191.

Hacquebard, P. A., Cameron, A. R., and Donaldson, J. R. 1965. A depositional study of the Harbour seam, Sydney Coalfield, Nova Scotia. Geological Survey of Canada, Paper 65-15.

Hamburg, G. 1984. Description of the Tracor Northern energy-dispersive system as applied to coal minerals analysis. Tracor Northern, Middleton, WI, Technology in Review, Vol. 2, Part 1, pp. 7–10.

Huggins, F. E., Kosmack, D. A., Huffman, G. P., and Lee, R. J. 1980. Coal mineralogies by SEM automatic image analysis. Scanning Electron Microscopy, **1980** (Part I): 532–540.

Huggins, F. E., Huffman, G. P., and Lee, R. J. 1982. Scanning electron microscope-based automated image analysis (SEM–AIA) and Mossbauer spectroscopy: quantitative characterization of coal

minerals. *In* Coal and coal products. American Chemical Society, pp. 239–258.

KWAK, T. A. P. 1968. Ti in biotite and muscovite as an indication of metamorphic grade in almandine amphibolite facies rocks from Sudbury, Ontario. Geochimica et Cosmochimica Acta, **32**: 1222–1229.

LASKOWSKI, J., BUSTIN, M., MOON, K. S., and SIROIS, L. L. 1985. Desulphurizing flotation of eastern Canadian high-sulphur coal. *In* Processing and utilization of high sulfur coals. *Edited by* Y. A. Attia. Elsevier, New York, pp. 247–266.

LEE, R. J., and KELLY, J. F. 1980. Overview of SEM-based automated image analysis. Scanning Electron Microscopy, **1980** (Part I), 303–310.

LEE, R. J., HUGGINS, F. E., and HUFFMAN, G. P. 1978. Correlated Mossbauer–SEM studies of coal mineralogy. Scanning Electron Microscopy, **1978** (Part I): 561–568.

MCCRONE, W. C., and DELLY, J. G. 1973. The particle atlas. 2nd ed. Ann Arbor Science Publishers, Ann Arbor, MI, pp. 1–194.

MILLOT, G. 1970. Geology of clays: weathering, sedimentology, geochemistry. Springer-Verlag, New York.

NEWMAN, W. R. 1935. Microscopic features of the Phalen seam, Sydney Coalfield, Nova Scotia. Canadian Journal of Research, **12**: 533–553.

NICHOLLS, G. D. 1968. The geochemistry of coal-bearing strata. *In* Coal and coal bearing strata. *Edited by* D. Murchison and T. S. Westoll. Elsevier, New York, pp. 269–307.

RAASK, E. 1985. Mineral impurities in coal combustion. Hemisphere Publishing Corp., London.

RUST, B. R., GIBLING, M. R., BEST, M. A., DILLES, S. J., and MASSON, A. G. 1987. A sedimentological overview of the coal-bearing Morien Group (Pennsylvanian), Sydney Basin, Nova Scotia, Canada. Canadian Journal of Earth Sciences, **24**: 1869–1885.

SKALA, W. 1979. Some effects of the constant-sum problem in geochemistry. Chemical Geology, **27**: 1–9.

STANTON, R. W., and FINKELMAN, R. B. 1979. Petrographic analysis of bituminous coal: optical and SEM identification of constituents. Scanning Electron Microscopy, **1979** (Part I): 465–472.

STRASZHEIM, W. E., and MARKUSZEWSKI, R. 1984. Automated image analysis of mineral matter in raw and supercleaned coals. Preprints of Papers — American Chemical Society, Division of Fuel Chemistry, **29**: 310–319.

——— 1985. Application of scanning electron microscopy and automated image analysis for characterization of mineral matter in coal. Preprints of Papers — American Chemical Society, Division of Fuel Chemistry, **30**: 47–55.

VLEESKENS, J. M., and HAMBURG, G. 1987. Coal mineral analysis "round-robin". ECN [Report] (Stichting Energieonderzoek Centrum Nederland), No. ECN-88-028.

WALSH, J. H., VISMAN, J., WHALLEY, B. J. P., and AHMED, S. M. 1969. Removal of pyrite from Cape Breton coals destined for use in metallurgical processes. *In* Mining, Processing and Extractive Metallurgy. 9th Commonwealth Mining and Metallurgical Congress. Institute of Mining and Metallurgy, London, Paper 35, pp. 143–177.

WELTON, J. E. 1984. SEM petrology atlas. American Association of Petroleum Geologists, Methods in Exploration Series.

WHITE, S. H., SHAW, H. F., and HUGGETT, J. M. 1984. The use of back-scattered electron imaging for the petrographic study of sandstones and shales. Journal of Sedimentary Petrology, **54**: 487–494.

ZODROW, E. L. 1980. Hydrated sulfates from Sydney Coalfield, Cape Breton Island, Nova Scotia, Canada: the Copiapite Group. The American Mineralogist, **65**: 961–967.

——— 1983. Some geochemical aspects of sedimentary rocks in proximity of coals, Sydney Coalfield (Upper Carboniferous), Cape Breton Island, Nova Scotia, Canada. International Journal of Coal Geology, **2**: 299–320.

ZODROW, E. L., and MCCANDLISH, K. 1980. Upper Carboniferous fossil flora of Nova Scotia. Nova Scotia Museum, Halifax.

ZODROW, E. L., WILTSHIRE, J., and MCCANDLISH, K. 1979. Hydrated sulfates in the Sydney Coalfield of Cape Breton, Nova Scotia. Pyrite and its alteration products. The Canadian Mineralogist, **17**: 63–70.

Appendix

TABLE A1. Coal-mineral weight percentage and size distribution for the Hub seam (Prince mine), collected beneath a sandstone roof

	Size distribution (% per bin)						CMA area (%)	CMA weight (%)
	0.2–1 μm	1–2.5 μm	2.5–5 μm	5–10 μm	10–20 μm	20+ μm		
Major								
Quartz	0	47	31	18	3	1	0.3	0.7
Kaolinite	31	31	24	13	2	0	6.0	7.7
Illite	55	26	13	4	1	0	5.0	3.2
Montmorillonite	0	45	49	5	1	0	0.1	0.1
Pyrite	24	23	29	16	6	2	8.2	61.4
Siderite	0	52	35	0	6	6	0.0	0.3
Calcite	0	35	23	12	19	12	0.0	0.5
Dolomite	0	0	100	0	0	0	0.0	0.0
Ankerite	0	0	0	0	50	50	0.0	0.1
Minor								
Gypsum	0	74	0	23	3	0	0.0	0.0
Halite	0	0	41	53	4	2	0.1	0.3
Sylvite	0	0	0	0	100	0	0.0	0.0
Rutile	0	46	54	0	0	0	0.0	0.0
Secondary								
Fe sulphate	15	10	15	17	20	22	0.3	6.1
Sulphur	88	7	4	1	0	0	0.5	0.1
Mixed								
Jarosite–pyrite	44	31	21	3	1	0	2.1	1.8
Mixed sulphate	78	10	8	4	0	0	0.4	0.1
Quartz–pyrite	85	9	4	1	0	0	6.7	1.8
Mixed silicate	64	19	11	4	1	1	6.3	6.6
Organic–quartz	89	9	2	0	0	0	19.9	1.6
Mixed chloride	95	1	2	1	0	0	1.1	0.1
Nonintegrated	78	18	3	1	0	0	37.1	6.8
Unknown	89	8	2	1	0	0	5.8	0.8
All minerals	71	17	8	3	1	0	100	100
No. of particles	295	1196	1821	779	1719	789	6599[a]	
No. of SEM fields	245		66		60		371[a]	
Magnification	500×		150×		50×			

NOTES: We analyzed 13 columnar benches, for a total of 6599 *in situ* mineral particles, using SEM–EDX–AIA on pelletized and polished coal-grain mounts. Summary of pooled output from CMA software.

[a]Total.

TABLE A2. CMA summary for columnar section of Harbour seam (Lingan mine), collected below a shale roof

	Size distribution (% per bin)						CMA area (%)	CMA weight (%)
	0.2–1 μm	1–2.5 μm	2.5–5 μm	5–10 μm	10–20 μm	20+ μm		
Major								
Quartz	48	32	14	5	1	0	3.9	3.1
Kaolinite	11	31	32	23	3	1	5.0	11.8
Illite	59	24	11	5	1	0	4.3	2.4
Montmorillonite	81	15	3	0	1	0	0.5	0.1
Pyrite	31	42	14	8	3	2	5.7	31.1
Siderite	0	0	26	31	22	21	0.2	7.0
Calcite	46	13	22	12	6	1	0.2	0.6
Minor								
Halite	0	0	50	33	12	5	0.0	0.2
Gypsum	0	0	0	0	0	100	0.0	0.0
Apatite	0	21	35	28	13	3	0.2	1.3
Rutile	0	0	83	0	17	0	0.0	0.0
Chlorite	26	34	26	11	2	0	3.2	4.6
Secondary								
Fe sulphate	94	1	1	2	1	1	2.1	3.6
Sulphur	0	71	15	13	0	0	0.0	0.0
Mixed								
Jarosite–pyrite	31	58	9	1	0	0	1.2	0.7
Mixed sulphate	61	38	0	0	0	0	0.1	0.1
Quartz–pyrite	88	9	2	0	0	0	11.8	1.0
Mixed silicate	48	30	14	6	2	1	11.9	15.6
Organic–quartz	76	17	6	1	0	0	8.5	1.4
Mixed chloride	0	0	69	30	1	0	0.0	0.1
Nonintegrated	63	30	5	1	1	0	26.6	9.5
Unknown	69	18	9	3	1	0	14.5	6.0
All minerals	60	25	10	4	1	0	100	100
No. of particles	193	943	1638	759	1607	695	5835[a]	
No. of SEM fields	230		85		94		409[a]	
Magnification	500×		150×		50×			

NOTE: Twelve benches (A–L (O omitted); see Table 3) analyzed, for a total of 5835 particles.
[a]Total.

TABLE A3. CMA summary for a bulk channel sample of Harbour seam (Donkin–Morien development)

	Size distribution (% per bin)						CMA area (%)	CMA weight (%)
	0.2–1 μm	1–2.5 μm	2.5–5 μm	5–10 μm	10–20 μm	20+ μm		
Major								
Quartz	0	31	49	14	6	1	0.3	1.0
Kaolinite	31	31	23	12	3	1	2.0	3.2
Illite	66	13	16	3	1	0	2.6	2.1
Montmorillonite	0	0	0	93	7	0	0.0	0.1
Pyrite	21	29	29	16	3	2	9.7	58.2
Siderite	0	0	0	0	62	38	0.0	0.3
Calcite	0	8	12	33	36	11	0.3	4.7
Minor								
Gypsum	0	0	100	0	0	0	0.0	0.0
Apatite	0	0	0	100	0	0	0.0	0.0
Rutile	0	0	0	0	100	0	0.0	0.0
Chlorite	0	0	0	100	0	0	0.0	0.1
Secondary								
Fe sulphate	0	23	22	28	18	9	0.2	2.1
Sulphur	72	23	5	0	0	0	0.5	0.1
Mixed								
Jarosite–pyrite	45	40	10	5	0	0	2.2	1.7
Mixed sulphate	31	31	22	15	1	0	0.2	0.2
Quartz–pyrite	83	9	5	3	0	0	2.6	1.3
Mixed silicate	43	30	17	5	4	1	1.3	2.8
Organic–quartz	94	4	2	0	0	0	20.9	1.4
Nonintegrated	82	11	4	3	0	0	54.2	19.1
Unknown	86	4	7	3	1	0	3.0	1.5
All minerals	75	12	7	4	1	0	100	100
No. of particles	131	550	623	377	628	313	2622[a]	
No. of SEM fields	110		18		20		148[a]	
Magnification	500×		150×		50×			

NOTE: Five pellets analyzed, for a total of 2622 particles.
[a]Total.

TABLE A4. CMA summary for columnar section of Phalen seam (Lingan mine), collected beneath shale

	Size distribution (% per bin)						CMA area (%)	CMA weight (%)
	0.2–1 μm	1–2.5 μm	2.5–5 μm	5–10 μm	10–20 μm	20+ μm		
Major								
Quartz	30	26	28	14	2	0	4.4	8.5
Kaolinite	60	16	12	11	2	0	5.6	7.2
Illite	69	19	7	4	1	0	9.8	6.7
Montmorillonite	73	12	9	5	1	0	0.7	0.5
Pyrite	17	45	22	12	3	1	7.7	36.2
Siderite	0	0	89	0	7	4	0.0	0.1
Calcite	20	10	20	35	11	5	1.1	9.4
Ankerite	0	0	100	0	0	0	0	0
Chlorite	21	28	30	18	3	0	0.1	0.2
Minor								
Halite	0	9	36	50	4	1	0.2	0.9
Apatite	0	78	13	0	7	2	0.0	0.1
Rutile	0	0	0	96	4	0	0.0	0.1
Secondary								
Fe sulphate	0	12	19	33	22	14	0.1	1.5
Sulphur	67	17	16	0	0	0	0.3	0.1
Mixed								
Jarosite–pyrite	48	38	11	3	0	0	2.4	2.2
Mixed sulphate	96	3	0	0	1	0	1.4	0.2
Quartz–pyrite	81	11	5	2	0	0	3.6	1.0
Mixed silicate	65	20	8	5	1	0	11.6	10.5
Organic–quartz	81	12	5	1	0	0	5.8	1.4
Mixed chloride	95	2	2	1	0	0	2.3	0.4
Nonintegrated	73	21	5	1	0	0	37.3	10.5
Unknown	79	11	7	3	0	0	5.7	2.5
All minerals	65	20	9	5	1	0	100	100
No. of particles	484	1822	2207	1199	2526	768	9006[a]	
No. of SEM fields	300		70		93		463[a]	
Magnification	500×		150×		50×			

NOTE: Seventeen pellets analyzed, for a total of 9006 particles.
[a]Total.

TABLE A5. CMA summary for columnar section of Gardiner seam (Novaco pit), taken beneath shale

	Size distribution (% per bin)						CMA area (%)	CMA weight (%)
	0.2–1 μm	1–2.5 μm	2.5–5 μm	5–10 μm	10–20 μm	20+ μm		
Major								
Quartz	46	30	17	5	2	0	8.5	4.4
Kaolinite	8	40	28	19	5	0	2.3	2.2
Illite	47	27	14	6	4	2	7.3	8.0
Montmorillonite	39	44	3	10	2	1	0.5	0.4
Pyrite	31	35	17	10	5	2	19.2	51.8
Siderite	0	0	62	21	11	7	0.2	1.2
Chlorite	0	0	0	91	9	0	0.0	0.1
Minor								
Rutile	0	0	100	0	0	0	0.0	0.0
Secondary								
Jarosite	0	0	0	0	100	0	0.0	0.1
Fe sulphate	0	15	5	9	32	39	0.3	7.0
Sulphur	0	0	100	0	0	0	0.0	0.0
Mixed								
Jarosite–pyrite	45	41	9	3	1	0	5.4	2.8
Mixed sulphate	67	21	6	6	0	0	0.3	0.0
Quartz–pyrite	72	20	5	2	0	0	16.7	4.2
Mixed silicate	72	13	9	5	2	1	13.5	7.2
Organic–quartz	87	10	2	0	0	0	17.6	0.9
Non-integrated	31	36	24	4	3	2	6.1	7.4
Unknown	40	35	16	4	3	2	2.0	2.3
All minerals	56	24	11	5	2	1	100	100
No. of particles	143	413	689	311	660	303	2519[a]	
No. of SEM fields	88		26		14		128[a]	
Magnification	500×		150×		50×			

NOTE: Five pellets analyzed, for a total of 2519 particles.
[a]Total.